Cryogenics 65 (2015) 49–58

Contents lists available at ScienceDirect

Cryogenics

journal homepage: www.elsevier.com/locate/cryogenics

Transient simulation of a miniature Joule–Thomson (J–T) cryocooler with and without the distributed J–T effect

R.M. Damle, M.D. Atrey *

Refrigeration and Cryogenics Laboratory, Department of Mechanical Engineering, Indian Institute of Technology (IIT) Bombay, Mumbai 400076, Maharashtra, India

ARTICLE INFO

Article history:
Received 20 August 2014
Received in revised form 18 October 2014
Accepted 27 October 2014
Available online 11 November 2014

Keywords:
J–T cryocooler
Transient
Distributed J–T effect
Heat exchanger

ABSTRACT

The aim of this work is to develop a transient program for the simulation of a miniature Joule–Thomson (J–T) cryocooler to predict its cool-down characteristics. A one dimensional transient model is formulated for the fluid streams and the solid elements of the recuperative heat exchanger. Variation of physical properties due to pressure and temperature is considered. In addition to the J–T expansion at the end of the finned tube, the distributed J–T effect along its length is also considered. It is observed that the distributed J–T effect leads to additional cooling of the gas in the finned tube and that it cannot be neglected when the pressure drop along the length of the finned tube is large. The mathematical model, method of resolution and the global transient algorithm, within a modular object-oriented framework, are detailed in this paper. As a part of verification and validation of the developed model, cases available in the literature are simulated and the results are compared with the corresponding numerical and experimental data.

1. Introduction

Miniature Joule–Thomson (J–T) cryocoolers are widely used for cooling of infrared sensors, cryosurgery probes, thermal cameras, etc. The main advantages of J–T type cryocoolers are: fast cool down time (of the order of seconds); simple design; no moving parts; high reliability; less maintenance; and low cost. The working medium for such cryocoolers is usually Nitrogen or Argon gas which is easily available at a reasonable price. The main parts of a J–T cryocooler are: storage vessel with high pressure gas; heat exchanger; expansion valve; and evaporator/load as shown in Fig. 1. The high pressure gas from the vessel after flowing through the heat exchanger expands through the expansion valve and cools because of the J–T effect. The cooling effect is extracted in the evaporator and thereafter, the gas flows through the low pressure side of the heat exchanger. The low pressure gas cools the high pressure gas on its way out to the atmosphere. This results in a heat exchanger with a counter-flow arrangement and is called a recuperative heat exchanger as it recovers the 'cold' from the return low pressure gas to cool the high pressure gas.

The working of the recuperative counter-flow heat exchanger directly affects the performance of the J–T cryocooler. The importance of a heat exchanger in cryogenic applications can be emphasized by the fact that it would need extremely high pressures (10^7 psia $\approx$ 689,475 bar) to liquefy nitrogen without a recuperative heat exchanger [1]. Flynn [2] demonstrated that a heat exchanger with 90% effectiveness is not sufficient to liquefy nitrogen for a cycle working between pressure limits of 1 bar and 100 bar. The effectiveness of the cryogenic heat exchangers needs to be as high as 97%. Atrey [3] observed that a drop in heat exchanger effectiveness from 97% to 95% reduced the liquid helium yield by 12%.

Being the most critical part of a cryocooler, the recuperative heat exchanger has been studied extensively by many authors. Xue et al. [4] and Ng et al. [5] have carried out steady state analysis of a miniature Hampson type heat exchanger with argon gas and compared it with their experimental data. An accurate geometrical model for the helical finned tube is included in the steady state thermodynamic model of the miniature heat exchanger by Chua et al. [6]. Hong et al. [7] used an effectiveness-NTU approach to predict the performance of the heat exchanger for pressures up to 500 bar with Argon and Nitrogen as working fluids. Recently, Ardhapukar and Atrey [8] presented a steady state analysis for the performance optimization of a miniature J–T cryocooler.

Chou et al. [9] reported transient numerical analysis along with experimental data for a miniature J–T cryocooler. Chien et al. [10] published a similar transient model where a self-regulating bellows mechanism was added, to the model of Chou et al. [9], to regulate the mass flow rate after reaching cryogenic temperatures. Hong et al. [11] carried out experiments to study the transient cool down characteristics of a miniature Joule–Thomson refrigerator

* Corresponding author. Tel.: +91 (22)2576 7522; fax: +91 (22)2572 6875.
E-mail address: matrey@iitb.ac.in (M.D. Atrey).

http://dx.doi.org/10.1016/j.cryogenics.2014.10.003
0011-2275/

Nomenclature

A	cross-sectional area, m^2
acf	area correction factor
CV	control volume
C_p	specific heat, J/kg K
D_{hel}	diameter of the helix, m
d_{fi}	inner diameter of the finned tube, m
dx	CV length, m
e_c	kinetic energy, m^2/s^2
e_r	emissivity of shield
f	fanning friction factor
G	mass velocity, kg/m^2 s
h	enthalpy, J/kg
k	thermal conductivity, W/m K
l	wetted perimeter, m
L	length of the finned tube/external annulus, m
m	mass, kg
$\dot{m}$	mass flow rate, kg/s
Pr	Prandtl number
p	pressure, N/m^2
Re	Reynolds number
$SLPM$	standard litres per minute
t	time, s
V	velocity, m/s
x	distance in positive x-direction, m
z	vertical distance in z-direction, m

Greek symbols

α	heat transfer coefficient, W/m^2 K
ϵ	precision for convergence
μ_{JT}	Joule–Thomson coefficient, K m^2/N
ρ	density, kg/m^3
ϕ	generic variable (p, T, V)
σ	Stefan–Boltzmann constant 5.67×10^{-8}, $W/m^2\ k^4$
τ_w	wall shear stress, N/m^2

Superscripts

$*$	guess value
0	value at previous time step

Subscripts

amb	ambient
c	cold gas in the external annulus
h	hot gas in the finned tube
ft	finned tube
in	inlet
m	mandrel
out	outlet
s	shield
si	inner surface of shield
so	outer surface of shield
w	finned tube wall
wi	inner surface of finned tube
wo	outer surface of finned tube
$(-)$	integral average over CV

using nitrogen gas at inlet pressures up to 120 bar. Hong et al. [12] also presented a numerical study of the operating characteristics of a miniature Joule–Thomson refrigerator.

Recently, Maytal [13] performed tests on four different constructions of Hampson type miniature J–T cryocoolers with mixed refrigerants. It was pointed out that the frictional pressure drop along the tube causes a distributed J–T expansion effect and any additional expansion device at the end of the tube can thus be eliminated. It was also suggested that the temperatures change due to the distributed J–T effect can be significant when the pressure drop along the flow of high pressure gas is substantial. He also commented on the aspects related to the modelling of this distributed J–T effect.

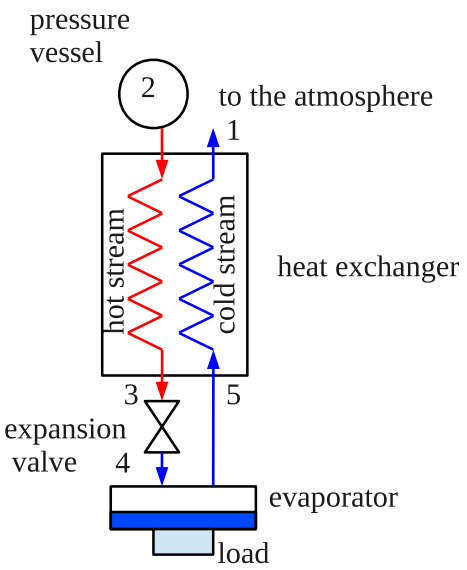

Fig. 1. Parts of a J–T cryocooler.

In general, transient numerical analysis has received less attention in the literature which is crucial for predicting the cool down characteristics of a miniature J–T cryocooler. Although the modelling of the time dependent accumulative (transient) terms in the continuity, momentum and energy equations are inherent to a transient formulation, Chou et al. [9] and Hong et al. [12] have neglected the accumulative terms for the continuity and momentum equations in their transient formulation. Also, the initial temperature and pressure maps for all the components of the heat exchanger at time $t = 0$, which are very important for the temporal evolution of the physical phenomenon, are not clearly mentioned. Moreover, previously presented numerical models, by Chou et al. [9], Chien et al. [10], Ng et al. [5], and Hong et al. [12], have modelled the J–T effect only at the outlet of the finned tube carrying the high pressure gas. They have not considered the distributed J–T effect along the length of the finned tube as pointed out by Maytal [13]. Thus, changes in the enthalpy of the fluid due to temperature alone (i.e., $dh = C_p dT$) have been considered along the tube length. This assumption may not be valid for the finned tube with a very large gradient of pressure along its length.

In this work, a one-dimensional transient model is developed for the recuperative heat exchanger of the J–T cryocooler. Time dependent terms are taken into account for the continuity, momentum and energy equations. To simulate the entire cryogenic cycle, as in a cryocooler, the J–T expansion process is also simulated to calculate the inlet temperature of the return gas in the external annulus. The so far neglected distributed J–T effect is also considered along the length of the finned tube where a huge

pressure drop (around 80–100 bar) is experienced by the fluid due to wall friction. Both temperature and enthalpy formulations are worked out to explore the distributed J–T effect. Physical properties are evaluated as a function of the local temperature and pressure. For different working conditions, the numerically obtained values of the outlet temperature of the fluid in the external annulus are compared with experimental data. The temperature profiles of the fluid streams over the heat exchanger length are also compared with available numerical data.

Also, an object-oriented and modular approach is employed for modelling the heat exchanger in this work. The heat exchanger is modelled as a collection of different basic elements; i.e., fluid streams, separating finned tube, mandrel and shield. These elements interact with each other only through boundary conditions. So, the method of resolution of each element can be different. This gives flexibility to choose models for individual elements as per requirement. From the software point of view, the program is reusable and easy to maintain.

2. Miniature J–T cryocooler configuration

The schematic diagram of a tube-in-tube counter-flow heat exchanger for a miniature Joule–Thomson cryocooler is shown in Fig. 2. The main parts of this heat exchanger are: a helical finned tube with high pressure gas, a mandrel over which the finned tube is wound, and a covering shield forming an external annular space for the returning low pressure gas. Normally, the high pressure gas enters the finned tube (hot side of the heat exchanger) at a pressure in the range of 100–400 bar depending on the working fluid. The temperature at the inlet is close to the ambient temperature (300 K). A very high pressure drop is experienced by the fluid in the helical finned tube along with heat transfer. The return gas in the external annulus (cold side of the heat exchanger) enters at low pressure around 1.5–2 bar and at an inlet temperature of about 80–110 K. The outer finned surface in the external annulus enhances the heat transfer to the return gas. The geometrical configuration of the heat exchanger (i.e., finned tube geometry, heat exchanger length, etc.) and the working conditions drastically affect the cool down characteristics. A numerical tool is therefore useful for the optimization of the geometrical and operating parameters of the heat exchanger.

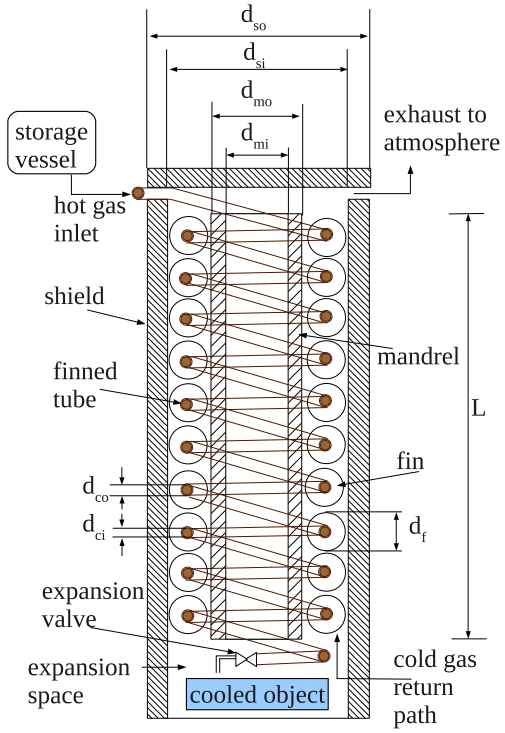

Fig. 2. Schematic of a miniature J–T cryocooler with the recuperative counter-flow heat exchanger.

3. Mathematical model

3.1. Control volume arrangement

In this work, a one-dimensional transient model is developed for the fluid streams and the solid elements (i.e., finned tube, mandrel and shield) which together form the heat exchanger. For the numerical resolution of the governing equations described in this section, it is first necessary to divide the different elements of the heat exchanger into a series of control volumes (CVs). The CV arrangements employed in this work for the finned tube, fluid in the finned tube and the fluid in the external annulus are shown in Fig. 3. For the finned tube, the nodes are placed at the centre of a CV while the nodes for the fluid streams are placed on the CV faces. The CV arrangement for the mandrel and the shield is the same as that of the finned tube. As the finned tube is helically wound on the mandrel, the total length of the tube is first calculated taking into account the pitch and diameter of the helix along with the vertical height (L) of the heat exchanger. This length can then be divided into any number of control volumes. The length of the fluid in the external annulus is also divided into a series of CVs which are of the form of annular rings.

In order to coincide the mesh pattern of the finned tube and inner hot fluid, same number of CVs are assigned to them. This is because the hot fluid and the finned tube, with same length, go together around the mandrel in a helical way. It is therefore convenient to associate each CV of high pressure fluid with the corresponding CV of the finned tube. The outer annular space with the low pressure fluid is a straight vertical column of height L. It can be divided into several CVs which can be different in number from the CVs of the finned tube. The number of CVs for the shield and the mandrel are the same as that for the outer annular fluid.

As the number of CVs of the finned tube and the inner fluid can be different as compared to the outer annular fluid, every finned tube CV is associated with its corresponding outer fluid CV. This association of tubes CVs is based on their height with respect to the height of outer fluid CVs. For example, as shown in the Fig. 4, the tube CVs with height less than z_1 are assigned to the first CV of the outer fluid. Similarly, other tube CVs are also associated with the outer fluid CVs. The surface area and perimeter of finned tube, and flow area and hydraulic diameter of the external annulus are calculated as in Ardhapurkar and Atrey [8].

3.2. Governing equations

3.2.1. Assumptions

The assumptions made in the derivation of the governing equations are:

(i) heat transfer and fluid flow is one dimensional along the length of solid and fluid elements of the heat exchanger;
(ii) axial conduction in the fluid is neglected;
(iii) body forces and axial stresses are negligible;
(iv) the helical tube is assumed to be perfectly circular and closely spaced;
(v) fin efficiency is assumed to be 100%;
(vi) diametrical clearance between fins and shield is neglected;
(vii) emissivity of the shield is assumed to be constant and receives outside radiation at ambient temperature.

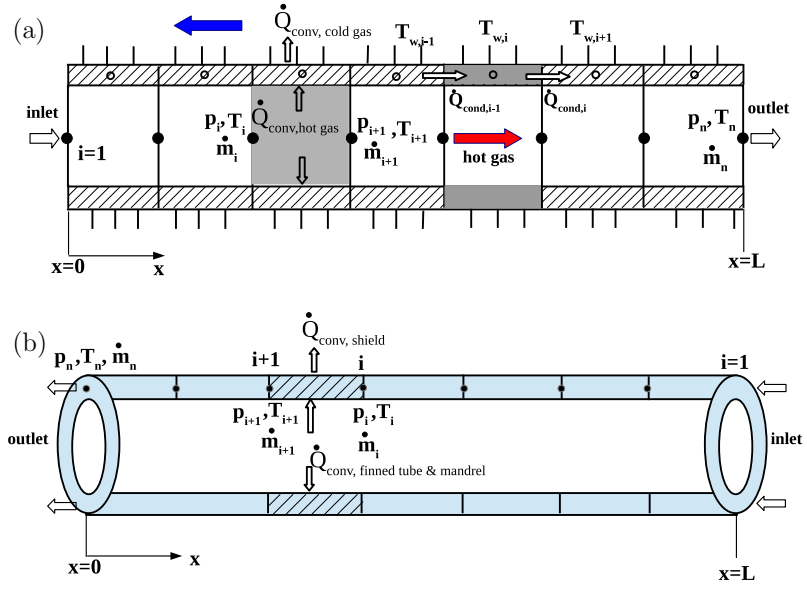

Fig. 3. Control volume arrangement: (a) finned tube and inner fluid and (b) outer fluid.

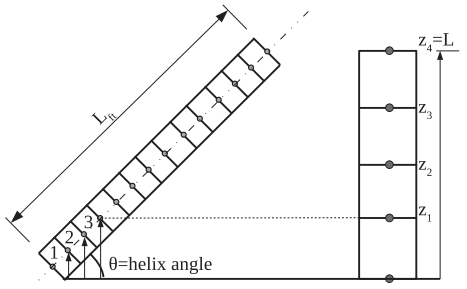

Fig. 4. Association of the finned tube CVs with annular fluid CVs.

(viii) The initial pressure of the fluid streams, at time $t = 0$, is assumed to be equal to the inlet pressure of the low pressure side (the pressure to which the high pressure gas expands).

3.2.2. Mass, momentum and energy conservation

The basic equations of conservation of mass, momentum and energy for the fluid elements and energy conservation equations for solid elements are written in a differential form. The mean properties of the fluid at the centre of the CV are calculated from the values at the nodes and are indicated with a overbar. The variables at the previous time step are indicated with a superindex '0'.

The conservation of mass over a fluid CV is:

$$A\frac{\partial\bar{\rho}}{\partial t}+\frac{\partial\dot{m}}{\partial x}=0 \tag{1}$$

The conservation of momentum is given by:

$$A\frac{\partial(\bar{\rho}\overline{V})}{\partial t}+\frac{\partial(\dot{m}V)}{\partial x}=-\frac{\partial p}{\partial x}\cdot A-\tau_w l_p \tag{2}$$

where $\tau_w = f\rho V^2/2$ is the wall shear stress, f is the Fanning friction factor, A is the cross-sectional area and l_p is the wetted perimeter.

Energy equation in terms of enthalpy is written as:

$$A\frac{\partial(\bar{\rho}\bar{h})}{\partial t}+\frac{\partial(\dot{m}h)}{\partial x}=\alpha\cdot l_p\cdot(T_w-\overline{T})+A\frac{\partial p}{\partial t}-\left(A\frac{\partial(\bar{\rho}\bar{e}_c)}{\partial t}+\frac{\partial(\dot{m}e_c)}{\partial x}\right) \tag{3}$$

Multiplying the mass conservation equation by $\bar{h}$, subtracting it from Eq. (3) and putting $dh = C_p dT - \mu_{JT} C_p dp$ according to Maytal [13] the energy equation in temperature form can be rearranged as:

$$A\bar{\rho}^0\overline{C}_p^0\frac{\partial\overline{T}}{\partial t}+\frac{\partial}{\partial x}\left(\dot{m}C_p(T-\overline{T})\right)=\alpha\cdot l_p\cdot(T_w-\overline{T})+A\frac{\partial p}{\partial t}-\left(A\frac{\partial(\bar{\rho}\bar{e}_c)}{\partial t}+\frac{\partial(\dot{m}e_c)}{\partial x}\right)+A\bar{\rho}^0\overline{C}_p^0\bar{\mu}_{JT}^0\frac{\partial p}{\partial t}+\frac{\partial}{\partial x}\left(\dot{m}C_p\mu_{JT}(p-\bar{p})\right) \tag{4}$$

Here, $\bar{\rho}^0$ is calculated at mean temperature $\overline{T}^0$ and mean pressure $\bar{p}^0$ while $\overline{C}_p^0$ and $\bar{\mu}_{JT}^0$ are evaluated at the mean temperature of $(\overline{T}+\overline{T}^0)/2$ and mean pressure of $(\bar{p}+\bar{p}^0)/2$. The last two terms in the energy equation with the temperature formulation (Eq. (4)) represent the distributed J–T effect or the changes in temperature due to variation of pressure. These terms are considered only for the fluid in the finned tube due the large pressure drop (around 80–100 bar) over its length.

The energy equations for the solid elements are the following:

Finned tube:

$$\rho_w A_w C_{pw}\frac{\partial T_w}{\partial t}=\frac{\partial}{\partial x}\left(k_w A_w\frac{\partial T_w}{\partial x}\right)+\alpha_h l_{wi}(\bar{T}_h-T_w)-\alpha_c l_{wo}(T_w-\bar{T}_c) \tag{5}$$

Mandrel:

$$\rho_m A_m C_{pm}\frac{\partial T_m}{\partial t}=\frac{\partial}{\partial x}\left(k_m A_m\frac{\partial T_m}{\partial x}\right)-\alpha_c l_m(T_m-\bar{T}_c) \tag{6}$$

Shield:

$$\rho_s A_s C_{ps}\frac{\partial T_s}{\partial t}=\frac{\partial}{\partial x}\left(k_s A_s\frac{\partial T_s}{\partial x}\right)-\alpha_c l_{si}(T_s-\bar{T}_c)-\sigma e_r l_{so}\left(T_s^4-T_{amb}^4\right) \tag{7}$$

3.3. Boundary conditions

The inlet temperature, pressure and mass flow rate are known for the gas in the finned tube. The same are known at the inlet of the return gas in the external annulus. All the solid elements (i.e.,

finned tube, mandrel and shield) are assumed to be adiabatic at ends. Thus,

$$at\ x=0\ \&\ t>0,\quad T=T_{h,in},\quad p=p_{h,in},\quad \frac{dT_w}{dx}=0,\quad \frac{dT_m}{dx}=0,\quad \frac{dT_s}{dx}=0 \tag{8}$$

$$at\ x=L\ \&\ t>0,\quad T=T_{a,e},\quad p=p_{c,in},\quad \frac{dT_w}{dx}=0,\quad \frac{dT_m}{dx}=0,\quad \frac{dT_s}{dx}=0 \tag{9}$$

$T_{a,e}$ is the temperature of the gas after isenthalpic expansion, from its state at the exit of the finned tube, to the pressure $p_{c,in}$ in the external annulus. This temperature goes on reducing from its initial value (ambient temperature) to cryogenic temperature $T_{c,in}$ at steady state. In addition, the initial temperature map for all the solid and fluid elements and pressure map for the fluid elements are specified as:

$$at\ t=0,\quad T^0=T_{amb},\quad p^0=p_{c,in}\quad for\quad 0\leqslant x\leqslant L \tag{10}$$

3.4. Heat transfer and friction factor correlations

The Fanning friction factor (f) for the flow through the helical finned tube, with the correlation of Timmerhaus and Flynn [14], is calculated as:

$$f=0.184\left(1+3.5\frac{d_{fi}}{D_{hel}}\right)Re^{-0.2} \tag{11}$$

The convective heat transfer coefficient (α_h) for the turbulent flow in the finned tube, calculated according to Timmerhaus and Flynn [14], is given by:

$$\alpha_h=0.023C_{ph}G_hRe^{-0.2}Pr^{-2/3}\left(1+3.5\frac{d_{fi}}{D_{hel}}\right) \tag{12}$$

The cold gas, on its way back to the atmosphere, exchanges heat by convection with the finned surface, outer surface of the mandrel and the inner surface of the shield. Reduction of flow area of the external annular region due to the finned tube is also considered according to Gupta et al. [15]. The convective heat transfer coefficient (α_c) for the return flow, with the correlation from Timmerhaus and Flynn [14], is estimated as:

$$\alpha_c=0.26C_{pc}G_cRe^{-0.4}Pr^{-2/3} \tag{13}$$

The Fanning friction factor (f) for the flow through the external annulus is calculated according to:

$$f=16/Re\ Re<2300 \tag{14}$$

$$f=0.079Re^{-0.25}\ Re>2300 \tag{15}$$

4. Numerical resolution

4.1. Modular object-oriented methodology

In this work, a modular object-oriented approach is employed for the numerical simulation of the counter-flow heat exchanger which forms the most of the cryocooler assembly. From the programming point of view in C++ basic classes for fluid and solid parts are identified and defined. Instantiations, called objects, can be derived from these basic classes to create individual elements of the heat exchanger, namely, the high pressure fluid, the low pressure fluid, the finned tube, the mandrel and the shield. For example, from a base '*Class*' called *Fluid* an object $f1$ can be created for the high pressure fluid in the finned tube as shown in Fig. 5. For the low pressure fluid in the external annular space a new '*Class*' with name *Fluid*2 is derived from the base class *Fluid*. The derived class inherits all the properties of the base class and in addition new features can be implemented. The advantage is that all the

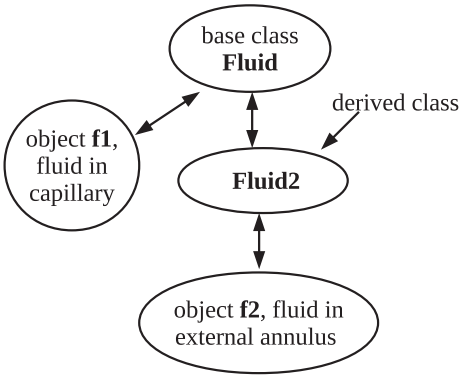

Fig. 5. Base and derived classes for the fluid elements.

functions and variables of the base class can be reused by the derived class and at the same time the internal method of resolution for both can be different. Now, from the derived class *Fluid*2, an object $f2$ is created for the return fluid in the external annulus. On the same lines, a finned tube object $t1$ is created from the base class *Tube*. Objects $s1$ and $m1$ are created from a base class *Annular – tube* representing the shield and the mandrel. These objects (elements) are then interlinked to form a thermal system (heat exchanger in this case) as shown in Fig. 6a.

All these objects solve themselves for given boundary conditions. These boundary conditions come from the neighbouring objects to which they are connected. For example, the $f1$ and $f2$ objects get the wall temperature from the object $t1$, while the $t1$ object receives fluid temperatures and heat transfer coefficients from the fluid objects $f1$ and $f2$. The advantage is that the method

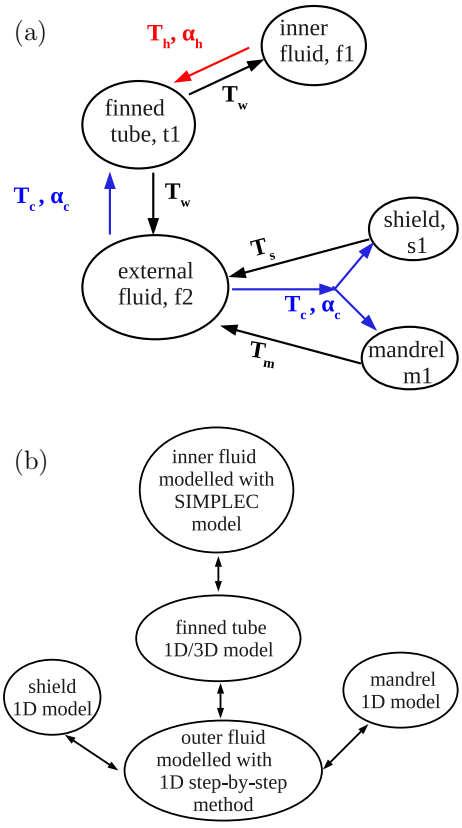

Fig. 6. Modular methodology: (a) modular heat exchanger and (b) different levels of modelling different elements in the same simulation.

of resolution of each element can be different (f1 can be solved with SIMPLEC algorithm [16] while f2 can resolved with a step-by-step method). Only the necessary boundary information (changing during the transient evolution) are fed to the concerned object. Thus, each element of the system can be modelled with different level of detail (see Fig. 6b) in the same simulation which gives flexibility to choose individual element models according to the desired accuracy. Moreover, new elements (classes in C++) and features can be added to already existing elements without changing basic framework. The program is thus reusable, easy to debug and also, easy to maintain.

4.2. Resolution of fluid and solid elements

Step-by-step method is employed for the resolution of the fluid streams in the finned tube and the external annulus. In the step-by step method, starting with the values of variables (e.g. p, T, $\dot{m}$) at a given cross-section i the respective values at the next cross-section $i+1$ are calculated. This method is suitable here because the pressure, temperature and mass flow rate at inlet cross-sections of both the finned tube and the external annulus are known and marching in the flow direction at each time step is possible to obtain the variable values at subsequent locations. The fluid CVs receive wall temperature from the surrounding CVs of the solid wall.

For the solid elements, integration of Eqs. (5)–(7) over a CV results in a system of linear algebraic equations. TDMA (Tri-Diagonal Matrix Algorithm) method is used for solving this system of equations. Heat transfer coefficients and fluid temperatures are received by the solid wall CVs from the fluid CVs in contact with them.

4.3. Global algorithm

The global resolution algorithm for the transient simulation of the cryocooler, modelled as a collection of different elements, is shown in Fig. 7. Geometrical parameters, initial map (at time $t = 0$) and boundary conditions are first set for each element of the heat exchanger. An iteration at a given time step consists of going to each element once and resolving the corresponding governing equations to get new value of variables (e.g., temperature, pressure and velocity). During an iteration, latest variable values from the linked elements are available to an element whose calculation is under process. For example, if the finned tube calculation is done after resolving both the fluid streams then the latest values of the fluid temperatures will be available for the heat transfer calculation of the finned tube wall.

After each iteration, at each CV, absolute or relative differences are evaluated between the new variable values and the variable values of the previous iteration. Each element calculates these differences at each of its CV and a maximum value from these calculated values is returned as the difference value for that element. A global maximum value (ϵ_{it}) is then found out from these individual element maximum values. This value, ϵ_{it}, represents the maximum absolute or relative difference for the entire heat exchanger for that iteration. If $\epsilon_{it} > \epsilon_{ts}$ (the convergence criteria set for every time step) iterations at the same time step are continued with updated variable values $\phi^* = \phi$. Time step calculation is over when the convergence criteria (i.e., $\epsilon_{it} < \epsilon_{ts}$) is achieved. Thereafter, the next time step calculation begins by updating the temporal map $\phi^0 = \phi$ of all variables. The process continues until the set steady state criteria, ϵ_{steady}, is reached.

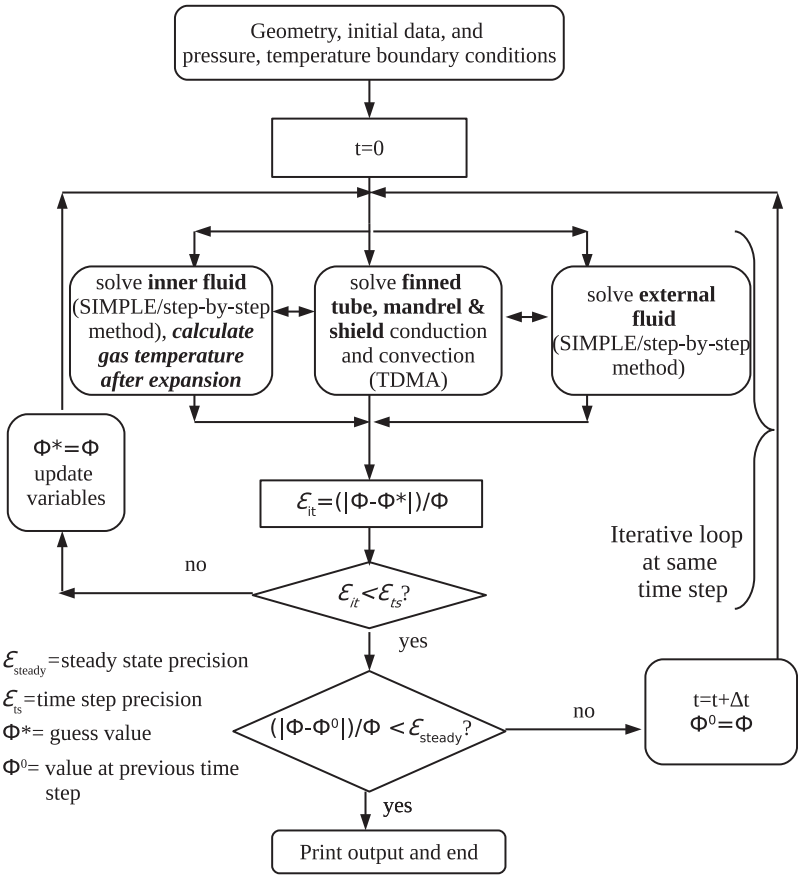

Fig. 7. Global resolution algorithm.

5. Results and discussion

In this work, cases published in the literature by Xue et al. [4] and Ng et al. [5] have been simulated and compared with the numerical model developed. The dimensions of a recuperative heat exchanger [5] and its components (i.e., finned tube, mandrel, etc.) are listed in Table 1. The operating parameters for these cases are listed in Table 2. Argon is used as the working fluid in all the cases. The properties of Argon as a function of temperature and pressure are obtained from the commercial software AspenONE [17]. At any given instant, for each CV, the physical properties like density, viscosity, specific heat, thermal conductivity and enthalpy are calculated as a function of temperature and pressure. The values of thermal conductivity, as a function of temperature, for the solid elements like finned tube, mandrel and shield are evaluated from the functions given by Ng et al. [5].

5.1. Convergence criteria and mesh requirement

The convergence at each time step is declared if the absolute differences of pressure, temperature and velocities are below 1×10^{-4}. Steady state is declared when the absolute differences for temperature and velocity, and relative differences of pressure are below to 1×10^{-3}. It is observed that at least 500 CVs are required on the high pressure fluid in the finned tube to meet the convergence criteria at each time step. Fig. 8 shows the evolution of the maximum absolute differences of temperature, pressure and velocity during a transient simulation. It can be seen that all these values are below 1×10^{-4} as per the set criteria. By keeping 500 CVs on the high pressure side, the number of CVs on the low pressure side are varied to see the effect of mesh refinement on different output parameters. Table 3 demonstrates that the temperature and pressure values at the exit of finned tube and external annulus do not vary with the number of CVs on the outer side. An additional case with 600 CVs for both inner and outer fluids shows that the variation with further mesh refinement is not significant.

5.2. The distributed J–T effect

In the literature, researchers [9,10,5,12] have modelled the changes in enthalpy of the high pressure fluid in the finned tube as a function of temperature only (i.e., $dh = C_p dT$ is assumed). Maytal [13] commented that the distributed J–T effect should be considered according to:

$$dh = C_p dT - \mu_{JT} C_p dp \tag{16}$$

Eq. (16) attributes the changes in enthalpy of the fluid not only to the temperature changes but also to the changes of pressure through the Joule–Thomson coefficient μ_{JT}. To explore whether the distributed J–T effect is significant, a tube without wall heat transfer is simulated. The case is simulated with the temperature formulation (Eq. (4)) with and without the terms for distributed J–T effect. Also, the same case is simulated with the enthalpy formulation (Eq. (3)) as it is expected to take care of the distributed J–T effect intrinsically. This is done to compare the results using both formulations and to cross check the way of implementation of the extra terms, representing the distributed J–T effect, in the temperature formulation. The inlet condition of pressure, temperature and mass flow rate for this case is the same as that for case A in Table 2. The tube diameter is taken equal to the inner diameter of the finned tube as given in Table 1. The steady state temperature profiles of the gas along the tube length are shown in Fig. 9. The frictional pressure drop over the length of the finned tube in this case is of the order of 100 bar. Without the term for distributed J–T effect, i.e., by assuming $dh = C_p dT$, temperature profile of the gas in the tube is a horizontal line of constant temperature. There is no change in temperature of the gas as there is no heat transfer. When the additional terms for distributed J–T effect ($\mu_{JT} C_p dp$) are considered in the temperature formulation, there is a substantial drop in temperature of the gas (around 30 K) even without wall heat transfer. The enthalpy formulation with no such extra term to account for distributed J–T effect also shows exactly the same decrease in temperature. This is because the distributed cooling effect has been inherent to the enthalpy formulation as expected. It is observed that the enthalpy remains constant during this process and therefore the term distributed J–T effect is appropriate for the cooling effect produced over the length of the tube. The temperature reduction for argon is large and demonstrates the distributed J–T effect in a

Table 1
Dimensions of the recuperative heat exchanger ([5]).

Geometrical parameters	Size
Inside diameter of finned tube, d_{fi}	0.3 mm
Outside diameter of finned tube, d_{fo}	0.5 mm
Inside diameter of mandrel, d_{mi}	2.3 mm
Outside diameter of mandrel, d_{mo}	2.5 mm
Inside diameter of shield, d_{si}	4.5 mm
Outside diameter of shield, d_{so}	4.8 mm
Length of recuperative heat exchanger, L	50 mm
Fin height, h_f	0.25 mm
Fin thickness, t_f	0.1 mm
Fin density, f_d	3.3 fins/mm
Helix diameter, D_{hel}	3.5 mm
Helix pitch, P_{hel}	1.0 mm

Table 2
Operating parameters of the test cases ([5]).

Case	Flow rate (SLPM)	$p_{h,in}$ (bar)	$T_{h,in}$ (K)	$p_{c,in}$ (bar)	$T_{c,in}$ (K)
A	10.145	140.47	291.94	1.3426	108.70
B	11.943	160.10	291.25	1.6362	109.90
C	13.927	179.12	291.49	1.7272	110.36

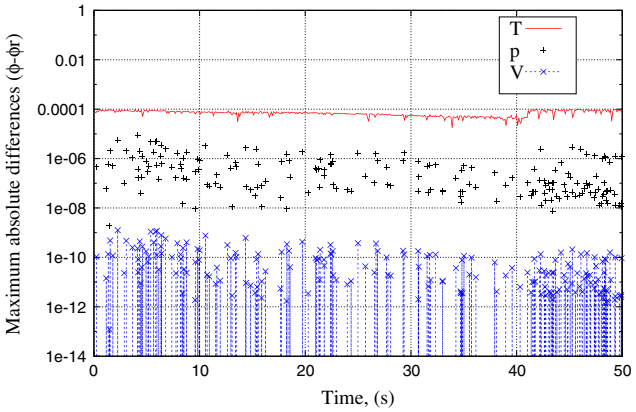

Fig. 8. Maximum differences at each time step for temperature, pressure and velocity (mesh: 500/100).

Table 3
Outlet parameters for case A with different meshes.

Sr. no.	Fluid CVs inner/outer	$T_{h,out}$ (K)	$p_{h,out}$ (bar)	$T_{c,out}$ (K)	$p_{c,out}$ (bar)
1	500/100	180.390	68.3582	285.785	1.16836
2	500/250	180.387	68.3549	285.789	1.16821
3	500/500	180.388	68.3549	285.789	1.16822
4	600/600	180.384	68.3618	285.791	1.16824

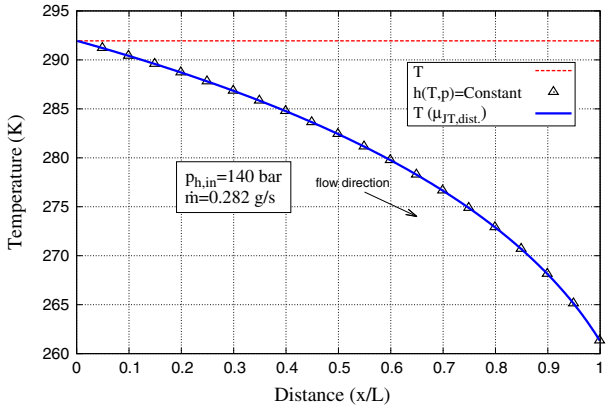

Fig. 9. Gas temperature profiles along the adiabatic tube with temperature formulation (T), enthalpy formulation ($h(T, p)$ = Constant), and temperature formulation with distributed J–T effect $\left(T\left(\mu_{JT,dist}\right)\right)$.

better way. This behaviour can be explained from the fact that for an ideal gas $dh = C_p dT$ as $\mu_{JT} = 0$. Thus, there is no cooling of the gas due to changes in pressure. On the other hand, for a real gas, below the inversion temperature, $\mu_{JT} > 0$ and cooling takes place due to the drop in pressure. Therefore, if pressure changes are large over the length of a tube, the cooling effect due to the distributed J–T effect cannot be neglected as suggested by Maytal [13]. The enthalpy formulation takes care of this effect intrinsically. In this work, the effect of this distributed cooling is studied for all the cases mentioned in Table 2.

5.3. Comparison of temperature profiles

Cases presented in Table 2 are simulated to test the numerical model developed in this work. The geometrical parameters of the heat exchanger are listed in Table 1. For these cases, Ng et al. [5] have published the numerically obtained temperature profiles for cases *A* and *C* under steady state conditions. These cases are simulated with the numerical model developed in this work. The simulations are carried out with and without the distributed J–T effect terms in the energy Eq. (4) with temperature formulation. The effect of applying an area correction factor to the outer surface area of the finned tube, as presented by Ardhapurkar and Atrey [8], is also studied.

As the program developed in this work is of transient nature, the steady state is obtained as consequence of transient evolution from initial conditions for these cases. The initial temperature map for all the elements is equal to the inlet temperature of the high pressure gas in the finned tube and the initial pressure is set as inlet pressure of the gas in the external annulus (i.e., $p_{c,in}$). At time $t > 0$, mass flow rate is imposed at the inlet cross sections of the finned tube and external annulus which are then resolved in the direction of flow with the step-by-step method considering the heat transfer interactions aforementioned.

The transient evolution of the temperature profiles of the hot and the cold fluid streams for case A are shown in Fig. 10. Initially, all the temperatures along the length of the inner and outer tubes are at the inlet temperature of the high pressure gas, i.e., at 291 K. It can be seen from Fig. 10 that the high pressure gas starts cooling due to the J–T effect and therefore the cold side inlet temperature starts decreasing. This, in turn, cools the gas in the finned tube. Subsequent expansions and heat exchange result in further lowering of temperatures of both the high pressure gas in the finned tube and the low pressure gas in the external annulus. This process continues until the temperature profiles of the hot and the cold

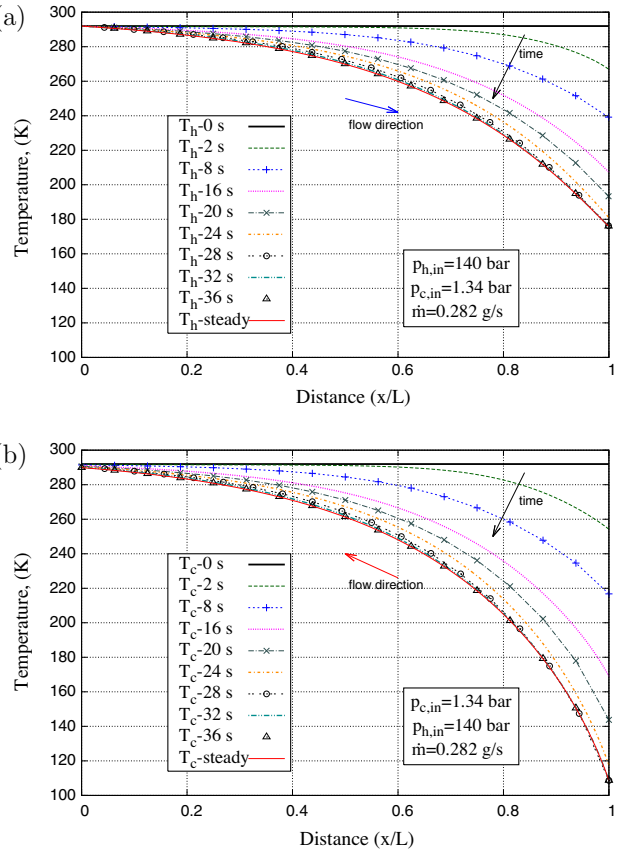

Fig. 10. Transient evolution of temperatures for case A: (a) gas in the finned tube and (b) gas in the annulus.

fluid do not change with time, i.e., when steady state is reached. It can also be seen, that after 36 s, the temperature profiles are practically unchanged and after 37.64 s the program terminates as the steady state criteria is achieved. Fig. 10 also shows that the criteria for declaring steady state is satisfactory.

The steady state temperature distributions for the case *A*, obtained as a consequence of transient evolution, are shown in Fig. 11. The temperature profiles of the hot and the cold fluid streams without the distributed J–T effect pass well over the numerical profiles predicted by Ng et al. [5]. As the predicted cold side temperatures are on the higher side, the hot side temperatures are also higher. Chua et al. [6] have mentioned that area correction factors were used by Xue et al. [4] and Ng et al. [5] to account for the reduction in the outer heat transfer area of the finned tube as it is spirally wound over the mandrel.

Ardhapurkar and Atrey [8], in their steady state analysis, also predicted higher temperatures on both hot and cold sides. Their profiles matched well with the profiles of Ng et al. [5] for an area correction factor (*acf*) of 0.7 for the outer surface area of the finned tube. They concluded that realistic area of the outer finned surface is necessary for correct numerical prediction. In this work also, the temperature profiles agree well for an *acf* of 0.7 without considering the distributed J–T effect. This in a way validates the present numerical analysis.

When the distributed J–T effect is taken into account, even without any correction factor to the outer surface of the finned tube, the hot side temperatures drop considerably and the temperature curve falls below the temperature profiles predicted by Ng et al. [5] and that with *acf* = 1.0. Lower temperatures on the hot side due to the distributed J–T effect also reduce the temperatures on the cold side due to lesser heat dissipation to the cold side

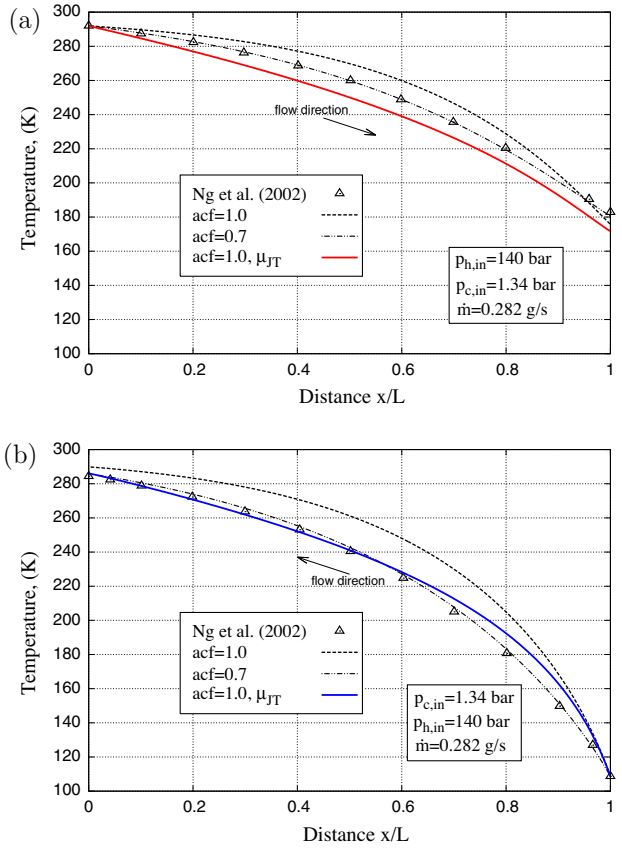

Fig. 11. Temperature distribution for case A: (a) gas in the finned tube and (b) gas in the annulus.

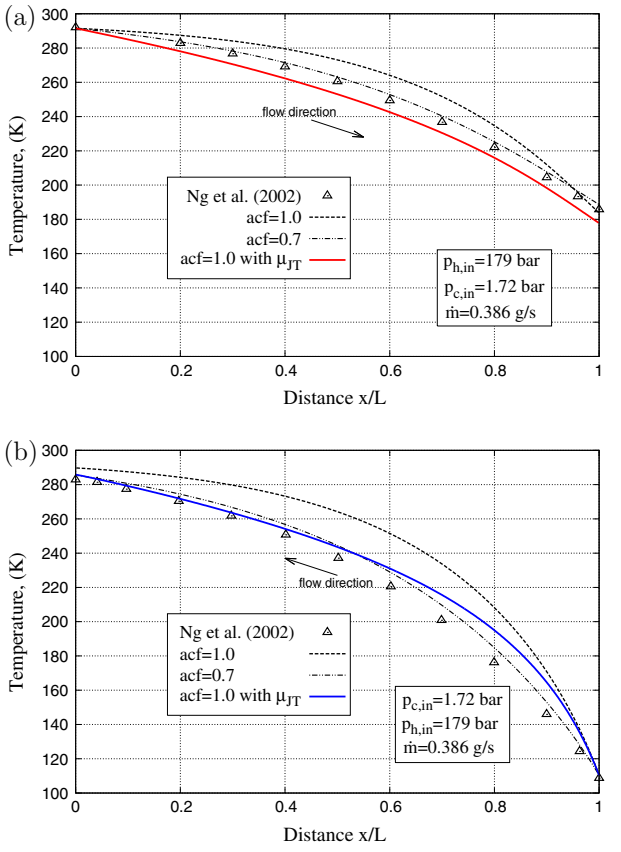

Fig. 12. Temperature distribution for case C: (a) gas in the finned tube and (b) gas in the annulus.

which further decrease the hot side temperatures. The temperature at the end of the finned tube is also lower with the distributed J–T effect. Similar observations are made for case C as shown in Fig. 12.

Area reduction with a correction factor leads to lesser heat dissipation to the cold side and in turn lower temperatures on both hot and cold sides. Although the effect of employing an *acf* is similar to considering the distributed J–T effect, the physical heat transfer interactions are different. It is quite possible that both these effects could be present in the actual working of the J–T cryocooler with different respective weightage. Also, the steady state temperature profiles given by Ng et al. [5] are their numerical predictions without the distributed J–T effect and with area correction factor. Comparison of the temperature profiles with experimental values along the length of the heat exchanger is necessary to understand the heat exchange process and whether any area correction factor is indeed required with the distributed J–T effect. It is though clear that with and without the distributed J–T effect, the temperature profiles are different and that the contribution of pressure drop in lowering the temperatures along the high pressure side cannot be ignored.

5.4. Model validation

Ng et al. [5] have also published the experimental values of the outlet temperature ($T_{c,out}$) of the gas in the external annulus for all the cases in Table 2. In this work the numerically obtained values of outlet temperature of the return gas in the external annulus are compared with the experimental data for all the three cases aforementioned. The comparison is shown in Table 4. The percent relative differences (% r.d.) between the numerical and experimental values are less than 2.6% for all the cases. The prediction of the outlet temperature of the return gas is in good agreement with the experimental data with *acf* = 0.7 and distributed J–T effect with no area reduction i.e., *acf* = 1.0. The relative differences are more for the cases without the distributed effect and *acf* = 1.0. Also, similar to the experimental observation, the outlet temperature is lesser for the highest inlet pressure with largest mass flow rate. Thus the model developed in this work is able to capture the trends and physics of the heat transfer and fluid flow phenomenon.

The cool down time for the different cases are shown in Table 5. It can be seen that the cool down time reduces with increase in inlet pressure as observed by Chou et al. [9]. Moreover, this decrease in the cool down time is observed for each column i.e., for *acf* = 1.0 and *acf* = 0.7 without the distributed J–T effect and *acf* = 1.0 with distributed J–T effect. This shows the consistent behaviour of the model developed. When the distributed effect is not considered, the cool down time is higher for *acf* = 0.7 than that for *acf* = 1.0. This is because with *acf* = 1.0 more heat is dissipated to the cold fluid as compared to *acf* = 0.7 due to larger area and due to lower temperature at the exit of the finned tube. Finally, with distributed J–T effect, the cool down time reduces further in all the three cases. This is due to the lower temperatures along the finned tube length and lower temperatures on the cold side with all the outer finned surface area available for heat transfer. The literature lacks to give more information about the geometrical configuration of the heat exchangers for miniature J–T cryocoolers. Cool down times are also not specified explicitly for a given configuration and operating conditions. Ng et al. [5] have mentioned in their work that steady state conditions were achieved in less than a minute for all the cases. Thus, the cool down time predicted in this work are realistic although individual case comparisons are necessary to fully validate the model.

Table 4
Numerical and experimental values of $T_{c,out}$ (working fluid: Argon).

Case	$p_{h,in}$ (bar)	Flow rate (SLPM)	Numerical values of $T_{c,out}$			$T_{c,out}$ Experimental (K)
			$acf = 1.0$ (K)	$acf = 0.7$ (K)	$acf = 1.0$, μ_{JT} (K)	
A % r.d.	140.47	10.14	289.865 (1.71)	285.791 (0.28)	286.063 (0.38)	284.98
B % r.d.	160.10	11.94	290.389 (1.97)	286.173 (0.49)	286.456 (0.59)	284.77
C % r.d.	179.12	13.93	289.734 (2.53)	285.461 (1.02)	285.825 (1.15)	282.57

Table 5
Cool down time with and without distributed J–T effect (working fluid: argon).

Case	$p_{h,in}$ (bar)	Cool down time (numerical)		
		$acf = 1.0$ (s)	$acf = 0.7$ (s)	$acf = 1.0$, μ_{JT} (s)
A	140.47	37.64	49.96	23.78
B	160.10	31.60	41.76	19.62
C	179.12	23.54	34.30	16.11

6. Conclusions

A transient model for the simulation of miniature J–T cryocoolers has been developed with a modular and object oriented approach for modelling the counter-flow recuperative heat exchanger. The heat exchanger is modelled as collection of basic elements linked with each other. Step-by-step algorithm is implemented for resolving mass, momentum and energy equations of the fluid streams. Realistic initial boundary conditions have been used for simulating the transient evolution. Axial heat conduction and convection at surfaces is considered for the solid elements like finned tube, mandrel and covering shield. Radiative heat transfer from the external surface of the shield is taken into account. Isenthalpic expansion process is also simulated to complete the cryogenic cycle. Physical properties are evaluated as a function of local temperature and pressure.

Traditionally, the numerical models on miniature J–T heat exchangers have attributed the changes in enthalpy of the fluid in the finned tube to changes in temperature only. The enthalpy changes due to variation of pressure, the distributed effect as suggested by Maytal [13], have been neglected. By carrying out simulations with enthalpy formulation and temperature formulation (with and without distributed J–T effect), it is shown that the changes of enthalpy, and therefore of temperature, due to variation in pressure along the length of the finned tube are significant and cannot be neglected when the pressure variations are large.

Steady state profiles, obtained as consequence of transient evolution, with area correction factor and without the distributed J–T effect match well with the numerical values of Ng et al. [5]. Higher temperature values on both hot and cold sides are predicted without the distributed J–T effect and no area correction. Considering the distributed J–T effect, even without area correction, lower temperatures of the hot and the cold sides are observed. The cool down time is also lower with the distributed J–T effect. The numerical values of the outlet temperature of the gas in the external annulus are in good agreement with the experimental values of Ng et al. [5] and the cool down times are also realistic. The model developed in this work is able to capture the heat transfer and fluid flow characteristics with physically realistic and consistent results.

Acknowledgements

The authors thank Mr. P.M. Ardharpukar, of S. S. G. M. College of Engineering, Shegaon – 444 203, India, for the techincal discussions about the work presented in this paper.

References

[1] Barron RF. Cryogenics systems. New York: McGraw-Hill book company; 1966.
[2] Flynn TM. Cryogenic engineering. 2nd rev. ed. New York: Marcel Dekker; 2005.
[3] Atrey MD. Thermodynamic analysis of Collins helium liquefaction cycle. Cryogenics 1998;38:1199–206.
[4] Xue H, Ng KC, Wang JB. Performance evaluation of the recuperative heat exchanger in on a miniature Joule–Thomson cooler. Appl Therm Eng 2001;21:1829–44.
[5] Ng KC, Xue H, Wang JB. Experimental and numerical study on a miniature Joule–Thomson cooler for steady-state characteristics. Int J Heat Mass Transfer 2002;45:609–18.
[6] Chua HT, Wang X, Teo HY. A numerical study of the Hampson-type miniature Joule–Thomson cryocooler. Int J Heat Mass Transfer 2006;49:582–93.
[7] Hong YJ, Park SJ, Choi YD. A numerical study of the performance of a heat exchanger for a miniature Joule–Thomson refrigerator. International Cryocooler Conference Cryocoolers, vol. 15; 2009. p. 379–86.
[8] Ardhapurkar PM, Atrey M. Performance optimization of a miniature Joule–Thomson cryocooler using numerical model. Cryogenics 2014;63:94–101.
[9] Chou FC, Pai CF, Chien SB, Chen JS. Preliminary experimental and numerical study of transient characteristics for Joule–Thomson cryocooler. Cryogenics 1995;35:311–6.
[10] Chien SB, Chen JS, Chou FC. A study on the transient characteristics of a self-regulating Joule–Thomson cryocooler. Cryogenics 1996;36:979–84.
[11] Hong YJ, Park SJ, Kim HB, Choi YD. The cool-down characteristics of a miniature Joule-Thomson refrigerator. Cryogenics 2006;46:391–5.
[12] Hong YJ, Park SJ, Choi YD. A numerical study on operating characteristics of a miniature Joule–Thomson refigerator. Supercond Cryogenics 2010;12:41–5.
[13] Maytal B-Z. Hampson's type cryocoolers with distributed Joule–Thomson effect for mixed refrigerants closed cycle. Cryogenics 2014;61:92–6.
[14] Timmerhaus KD, Flynn TM. Cryogenic process engineering. New York, USA: Plenum press; 1989.
[15] Gupta PK, Kush PK, Tiwari A. Design and optimization of coil finned-tube heat exchangers for cryogenic applications. Cryogenics 2007;47:322–32.
[16] Patankar SV. Numerical heat transfer. Hemisphere Publishing Corporation; 1980.
[17] AspenONE V 7.1. Aspen Technology Inc., Burlington, MA 01803, USA; 2009.